Simulation and optimisation of spiral-wound reverse osmosis process for the removal of N-nitrosamine from wastewater

Simulation and optimisation of spiral-wound reverse osmosis process for the removal of N-nitrosamine from wastewater

M. A. Al-Obaidi [1, 2], C. Kara-Zaïtri [1] and I. M. Mujtaba [1, *]

[1] Chemical Engineering Division, School of Engineering, University of Bradford, West Yorkshire BD7 1DP, UK
[2] Middle Technical University, Iraq – Baghdad
*Corresponding author, Tel.: +44 0 1274 233645
E-mail address: I.M.Mujtaba@bradford.ac.uk

Abstract

N-nitrosamine in wastewater treatment processes can contribute to several public health impacts including human carcinogens even at very low concentration. In this work, spiral-wound reverse osmosis (SWRO) process is used to remove N-nitrosamine compounds from wastewater. Effects of operating parameters of the SWRO process on the removal of N-nitrosamine, total water recovery, and specific energy consumption for a SWRO configurations are evaluated via simulation and optimisation. For this purpose, the one-dimensional distributed model developed earlier by the authors is modified by including different mass transfer coefficient correlation, temperature dependent water and solute permeability correlations and energy equations. The model is first validated by estimating a new set of model parameters using eight set of experimental data from the literature and is then used to simulate the process with and without energy recovery device to facilitate deeper insight of the effect of operating conditions on the process performance. The model is then embedded within an optimisation framework and optimisation problems to maximise N-nitrosamine rejections and to minimise specific energy consumption are formulated and solved while the operating conditions are optimized simultaneously.

***Keywords*:** Reverse Osmosis; Spiral-wound Module; One-dimensional Modelling; Optimisation; N-nitrosamine Removal; Energy Consumption.

1. Introduction

N-nitrosamine is considered as one of the by-products of disinfection process of secondary-treated wastewater effluent with chloramines, chlorines and ozone (Bond et al., 2011). Also, the International Agency for Research on Cancer has classified N-nitrosamine as possible human carcinogen where a cancer risk level is exhibited at 0.7 ng/l concentration (US EPA, 2009a). N-nitrosamine (especially NDMA, N-nitrosodimethylamine-D6) has been detected above established limits in treated water supply systems including drinking water and wastewater facilities. Therefore, many water authorities around the globe have been regulated against an allowable N-nitrosamine concentration level in drinking water and recycled water intended for potable consumption (US EPA, 2009b). The removal of N-nitrosamine from water and wastewater has been achieved using several approaches such as UV/H_2O_2 oxidation, photolytic degradation, photocatalytic oxidation, chemical oxidation, adsorption on resin and zeolites and membrane technology (Sharma, 2012). Sharma (2012) has reviewed many N-nitrosamine treatment processes and illustrated the specification of each one. It is concluded that resin and zeolites adsorption, activated carbon adsorption, sand filtration and ozonation have a little effect in removing NDMA (Krauss et al., 2010). Also, the possibility of formation of undesirable compounds as by-products including NDMA is valid after chlorinating the ultraviolet-treated water (Miyashita et al., 2009). Moreover, all the advanced technologies require high energy and are therefore expensive (Steinle-Darling et al., 2007; Sharma, 2012; Fujioka, 2014).

However, Reverse Osmosis is not only a significantly cheaper solution in terms of energy consumption in water desalination and wastewater treatment process, but also can achieve the stringent limits of undesirable particles and pollutants, which are likely to increase in the future (Marcovecchio et al., 2005; Akin and Temelli, 2011; Reverberi et al., 2014). Furthermore, spiral-wound RO modules are less susceptible to membrane fouling (compared to hollow fiber module) and are easier to clean and the cost of filtration has decreased significantly due to the improvements made in membrane manufacturing materials in recent years (Butt et al., 1997; Wagner, 2001). However, the energy consumption contributes most to the operating cost of the RO filtration process despite the promotion of efficient and reliable high-pressure pumps and power recovery turbines. This is due to the requirement of operating the process at high pressure to overcome the osmotic pressure (Song et al., 2002; Geraldes et al., 2005; Qi et al., 2012).

The performance of the RO process is quite sensitive to many design and operating conditions as demonstrated in several RO simulation and optimisation studies (Villafafila and Mujtaba, 2003; Abbas, 2005; Sassi and Mujtaba, 2013). Turbines and pressure exchangers options are used in the optimisation solution of Villafafila and Mujtaba (2003), who have reduced energy consumption by up to 50%.

In wastewater treatment, Madaeni et al. (2006) studied the operating parameters of trans-membrane pressure, temperature, and concentration, which influence the total flux and rejection of a solution containing nitrate, nitrite, sulfite and phosphate using SWRO pilot-plant. The optimisation results showed that trans-membrane pressure and temperature cause the highest impact on water flux in comparison to the feed concentration while the solute rejection is extremely affected by the feed concentration with a minor contribution for both the feed pressure and temperature. Sannino et al. (2013) identified the critical feed operating pressure, which keeps a constant permeate flow rate. This yields a short-term inhibit fouling in the batch process of a pilot-scale plant of two spiral-wound nano-filtration and reverse osmosis membranes supplied by Osmonics. Most recently Al-Obaidi et al. (2017a) studied Genetic Algorithm based optimisation in RO process for the removal of chlorophenol from wastewater.

To the best of the authors' knowledge, the development of a spiral-wound RO model based on the Spiegler and Kedem concepts and its validation for N-nitrosamine compounds have only been explored by Fujioka et al. (2014). A maximum rejection of eight N-nitrosamine compounds between 62% and 99% has been obtained by the experiments at 10.1 atm pressure, 2.43E-3 m^3/s of feed flow rate and 20 ºC temperature. However, no previous studies focussed on the analysis of the energy consumption of RO process for the removal of N-nitrosamine from wastewater. Also, the optimisation of the RO process for the removal of N-nitrosamine has not been considered yet.

Therefore, in this work, first we provide the full analysis of the energy consumption of the RO process via simulation. For this purpose, a modified model developed earlier by Al-Obaidi et al. (2017b) will be used. The modified model considers the impact of temperature on the transport parameters and incorporates additional equations specific to energy consumption of high-pressure pump, boiler, and energy recovery devices. The new model will be validated using the published experimental data of eight N-nitrosamine solutes of Fujioka et al. (2014). The impacts of operating parameters on N-nitrosamine rejection, water recovery, and energy consumption for two RO process configurations are presented in detail which have facilitated optimisation problem formulation with feasible bounds on constraints within gPROMS. Finally, two optimisation problems are formulated and solved, one to maximise the N-nitrosamine rejection and the other to minimise the energy consumption of the process.

2. Previous experimental work of Fujioka et al. (2014)

A pilot-scale cross-flow RO filtration system of three 4″ glass-fiber pressure vessels (Fig. 1) used by Fujioka et al. (2014) consists eight N-nitrosamine solutes with a molecular weight in the range of (74 – 158 g/mol) as summarised in Table 1. The N-nitrosamine stock solution containing 10 mg/L of each N-nitrosamine solutes [N-nitrosodimethylamine-D6 (NDMA), Nnitrosomethylethylamine-D3 (NMEA), N-nitrosopyrrolidine-D8 (NPYR), N-nitrosodiethylamine-D10 (NDEA), N-nitrosopiperidine-D10 (NPIP), N-nitrosomorpholine-D8 (NMOR), N-nitrosodipropylamine-D14 (NDPA) and N-nitrosodi-n-butylamine-D9 (NDBA)] were prepared in pure methanol. Also, aqueous feed stock solutions of NaCl, $CaCl_2$ and $NaHCO_3$ were prepared in Milli-Q water at 2M (NaCl) and 0.1 M ($CaCl_2$ and $NaHCO_3$) concentrations to mimic the background electrolyte composition typically found in the secondary or tertiary treated wastewater. The stock solution of N-nitrosamine compounds is mixed with the aqueous feed stock solution to obtain approximately 250 ng/L of each target Nitrosamine compound in the feed to the RO process (Fujioka, 2014). The inlet concentrations of all N-nitrosamine solutes are given in Table 1.

The feed tank (0.3 m^3) in Fig. 1 was filled in with the model wastewater (as described above) at the beginning of the process. After the process being started the concentrate and permeate streams are collected back in the feed tank to maintain a constant feed concentration. The experimental work of Fujioka et al. (2014) has considered a very low concentration of N-nitrosamine. Therefore, the physical properties of diffusivity, density and viscosity have been assumed identical to water equations and are calculated using Eqs. (14 - 17) (Appendix A in Table A.1). Each pressure vessel holds only one spiral-wound element and are linked in series.

The feed was pumped using a pump type (CRN 3-25, Grundfos, Bjerringbro, Denmark) at constant volumetric flow rate of 2.43×10^{-3} m^3/s, while the average permeate flux was adjusted at 2.78×10^{-6}, 5.56×10^{-6} and 8.33×10^{-6} m/s during the experiments by increasing the operating feed pressure from 4, 6.5 and 10.1 atm respectively. The feed temperature was controlled at 20±0.1 °C along the experiments (Fujioka, 2014).

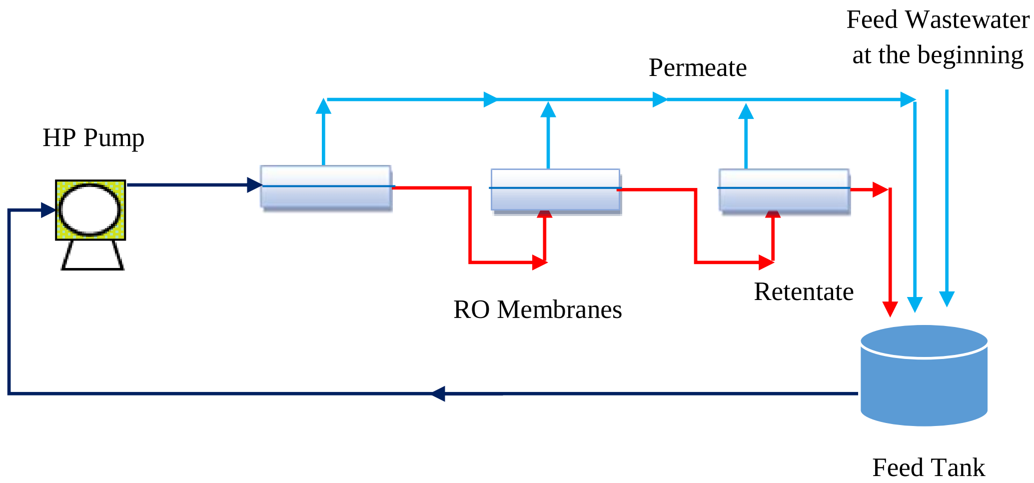

Fig.1. Schematic diagram of the pilot-scale plant used by Fujioka et al. (2014)

Table 1. Physical and transport parameters of the eight N-nitrosamines (Fujioka et al., 2014)

Name	Molecular weight (g/mol)	Inlet feed concentration, $C_{s(0)}\ x10^9$ (kmol/m³)	Solute permeability coefficient, B_s (m/s) at 20 °C	Reflection coefficient, σ (dimensionless)
NDMA	74.05	3.3761	$5.35x10^{-6}$	0.953
NMEA	88.06	2.8389	$1.14x10^{-6}$	0.958
NPYR	100.06	2.4985	$5.12x10^{-7}$	0.973
NDEA	102.08	2.4490	2.2610^{-7}	0.985
NPIP	114.08	2.1914	9.2510^{-8}	0.993
NMOR	116.06	2.1540	2.0610^{-7}	0.991
NDPA	130.11	1.9214	6.0210^{-8}	0.992
NDBA	158.14	1.5808	4.3310^{-8}	0.990

3. Proposed Spiral Wound RO configuration

Fig. 2 shows the proposed configuration of RO configuration of this study. The main addition to this configuration compared to the configuration of Fig. 1 are the existence of the high-pressure pump HPP, booster pump BP, energy recovery device ERD, and the feed tank boiler (electric) as we wanted to study the impact of feed temperature on the solute rejection. The feed tank is filled with wastewater (with the same specification as considered by Fujioka et al. (2014). The first run is carried out at a reference temperature T_{Ref} of 20 °C followed by boiling the feed tank from 20 to 22 °C in one hour. Then, another treatment is carried out at the new temperature (22 °C). This is followed by a series of several runs which are carried out in a step change of 2 °C for each run till 44 °C. Note that the maximum operating temperature of the membrane selected is 45 °C (Table 4).

The tank feed flow rate $F_{b(Tank)}$ is split into two fractions towards ERD ($F_{b(ERD)}$) and HPP ($F_{b(HPP)}$) at atmospheric pressure P_{atm}. While, the total permate $F_{P(Total)}$ at atmospheric pressure and the retentate are collected in the feed tank as in Fig. 1 to maintain a constant feed concentration. The total rejected brine $F_{b(L)}$ discharged from the last module is 100% recycled to ERD with high pressure $P_{b(L)}$ to pressurise the feed entering ERD. More specifically, the importance of ERD is to transfer the energy from the high-pressure brine stream by recovering the surplus pressure and delivering it directly to the incoming feed stream, which reduces the energy consumption of the RO process by recycling the brine energy (Anderson et al., 2009). The pressure losses in the membrane module will be compensated by BP (Greenlee et al., 2009). Then, the feed flow rate of HPP ($F_{b(HPP)}$) and BP

($F_{b(ERD)}$) are collected to form the inlet feed flow rate of reverse osmosis unit $F_{b(0)}$ with the inlet feed pressure $P_{b(0)}$. The performance of process rejection and recovery will be estimated by specifying the total permeate concentration and flow rate of the plant permeate stream. Moreover, the calculations of the specific energy consumption will be carried out for both configurations of the RO pilot-plant with and without ERD (Figs. 1 and 2).

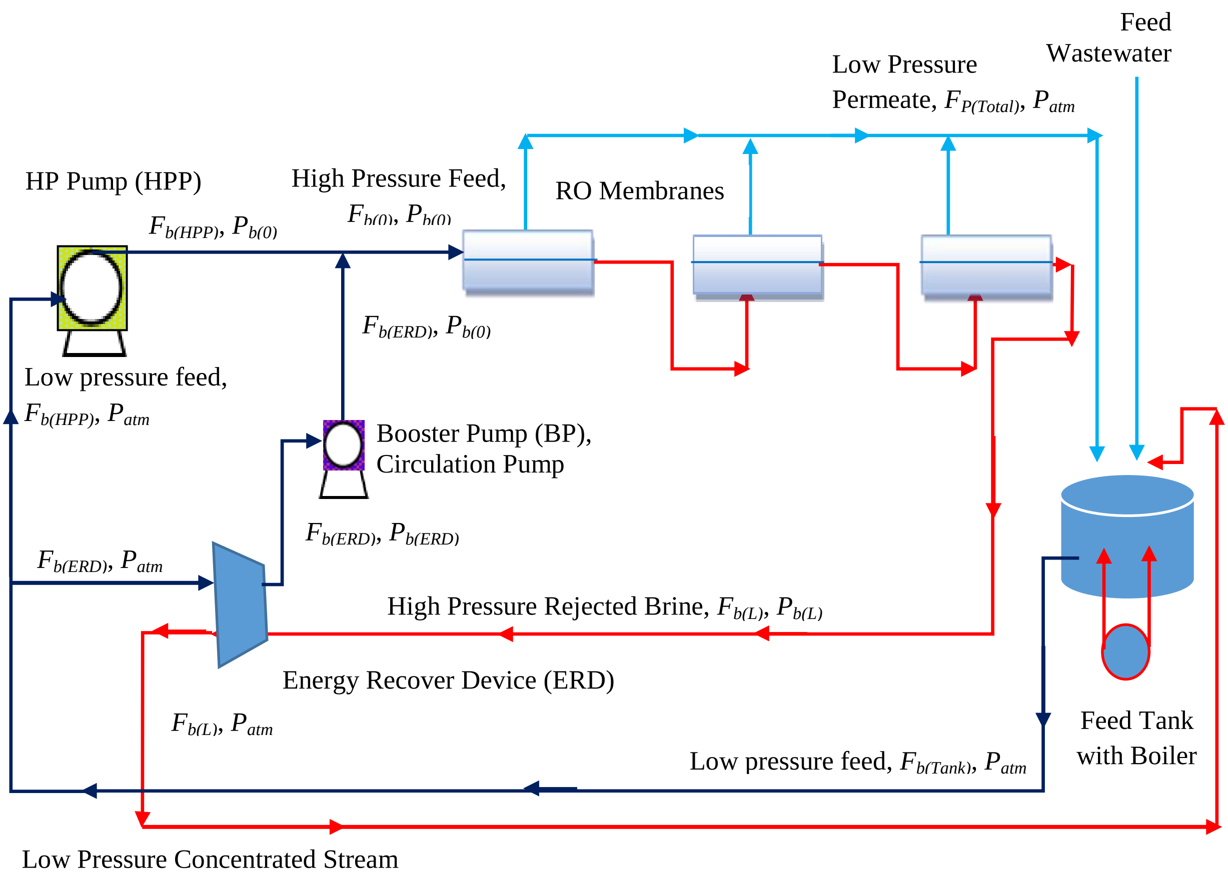

Fig. 2. Schematic diagram of a conventional RO pilot-scale plant

4. Process Model

4.1. Assumptions

The mathematical model is based on the following assumptions.

1. The membrane is made up of flat channels and spacers with neglecting the curvature of the channel.
2. Validity of the Spiegler-Kedem model for the transport of water and solute through the membrane (Spiegler and Kedem, 1966).
3. Validity of Darcy's law concerning the pressure drop in porous media where the friction parameter is used to characterise the pressure drop.

4. The film theory quantifies the concentration polarisation.
5. The permeate pressure is constant and equal to 1 atm.
6. A constant solute concentration is assumed in the permeate channel and the average value will be calculated from the inlet and outlet permeate solute concentrations.
7. The model is investigated for simply one-dimensional transport (x- coordinate).
8. The underlying process is assumed to be isothermal. Therefore, the temperatures of the feed, brine, and permeate are equal.
9. Constant pump and energy recovery device efficiencies. This is to quantify the efficiency of HPP and ERD.

4.2. Model Equations

Based on the above assumptions (1-8) Al-Obaidi et al. (2017b) described the transport phenomena of water and solute through the membrane module and to simulate the performance of N-nitrosamine compounds rejection using a spiral-wound RO membrane module. Their model equations are given in Appendix A, Table A.1. In this work, following equations required are added to the original model thus giving the modified model.

The mass transfer coefficient along the x-axis $k_{(x)}$ was estimated using the empirical correlation of Senthilmurugan et al. (2005) of Eq. (1).

$$k_{(x)} = 0.753 \left(\frac{K}{2-K}\right)^{0.5} \left(\frac{D_{b(x)}}{t_f}\right) \left(\frac{\mu_{b(x)}\, \rho_{b(x)}}{D_{b(x)}}\right)^{0.1666} \left(\frac{2\, t_f^{\,2}\, U_{b(x)}}{D_{b(x)}\, \Delta L}\right)^{0.5} \tag{1}$$

Furthermore, the effects of temperature variation on both water permeability L_p and solute permeability B_s coefficients are described in Eqs. (2) and (3) respectively as used by Sarkar et al. (2008).

$$L_{p(T_b+273.15)} = L_{p(T_0+273.15)} \frac{\mu_{b(T_o+273.15)}}{\mu_{b(T_b+273.15)}} \tag{2}$$

$$B_{s(T_b+273.15)} = B_{s(T_o+273.15)} \frac{T_b+273.15}{T_o+273.15} \frac{\mu_{b(T_o+273.15)}}{\mu_{b(T_b+273.15)}}$$

(3)

where T_0 is the reference temperature of 20 °C. Moreover, the specific energy consumption $E1$ of RO filtration system used by Fujioka et al. (2014) is calculated using Eq. (4) of Qi et al. (2012) based on the use of only a high-pressure pump. Here, $P_{b(0)}$ in atm and $E1$ in kWh/m³.

$$E1 = \frac{\frac{\left(\left(P_{b(0)}101325\right)F_{b(0)}\right)}{F_{p(Total)}\,\varepsilon_{pump}}}{36x10^{5}} \quad (4)$$

The calculation of the specific energy consumption for the conventional configuration of RO filtration system $E2$, which consists of a high-pressure pump (HPP), booster pump (BP) and energy recovery device (ERD) is carried out using Eq. (5). More specifically, the energy performance of the conventional pilot-plant is analysed based on the outgoing and ingoing entering energies. One of the aims of this paper is to determine the energy consumption due to its major contribution in total filtration cost, and which can reach values as high as 45% (Zhu et al., 2009).

$$E2 = \frac{\frac{\left(P_{b(0)}\,101325\right)F_{b(0)}}{F_{p(Total)}\,\varepsilon_{pump}} - \frac{\left(P_{b(L)}\,101325\right)F_{b(L)}\,\varepsilon_{ERD}}{F_{p(Total)}}}{36x10^{5}}$$

(5)

Eq. (6) calculates the outlet pressure of ERD $P_{b(ERD)}$ regarding the outlet pressure of membrane modules $P_{b(L)}$.

$$\varepsilon_{ERD} = \frac{P_{b(L)}}{P_{b(ERD)}}$$

(6)

For the case where the temperature of the feed tank is raised using a boiler, the heat supplied Q (j/s) by the boiler is calculated using Eq. (7) with T_{Ref} = 20 ºC. The boiler energy consumption $E3$ (kWh/m³ of permeate) is calculated using Eq. (8), while the total energy consumption $E4$ (kWh/ m³ of permeate) is calculated using Eq. (9), taking into account the energy consumption of the HPP and boiler in addition to the gain of energy using ERD.

$$\frac{d\left(T_{Tank} - T_{Ref}\right)}{dt} = \frac{Q}{\rho\, C_p\, V}$$

(7)

where (ρ, C_p and V) are the density of water (kg/m³), specific heat capacity of water (j/kg K) and volume of feed tank (m³) respectively.

$$E3 = \frac{\left(Q/F_{p(Total)}\right)}{36x10^{5}}$$

(8)

$$E4 = E2 + E3$$

(9)

The process model presented in Appendix A in Table A.1 and Eqs. (1 – 9) can be written in the following compact form:

$$f(z, x(z), x^{-}(z), u(z), v) = 0; \quad [z_0, z_f] \quad (10)$$

Where, z is the independent variable (length of membrane), $x(z)$ is the set of all differential and algebraic variables, $x^{-}(z)$ represents the derivative of $x(z)$ with respect to length of membrane, $u(z)$ is the control variables and v denotes the constant parameters of the process. The membrane length under consideration [z_0, z_f] and function f are assumed to be continuously differentiable with respect to all their arguments.

5. Determination of transport parameters

Experimental data of Fujioka et al. (2014) is used to estimate unknown transport parameters of the process model. The unknown parameters of the model are water permeability coefficient L_p, solute transport parameter $B_{s,}$ the reflection coefficient σ and friction parameters b. The membrane transport parameters B_s and the reflection coefficients σ of the eight selected N-nitrosamine solutes are assumed to be constants (Table 1) and taken from Fujioka et al. (2014) who considered a constant feed flowrate. Note, Murthy and Gupta (1999) proved a nearly constant solute transport parameter and reflection coefficient for the experiments of Sodium Cyanide-water system using a commercial thin film composite polyamide membrane at a range of feed flow rate 300 to 900 ml/min. However, Fujioka et al. (2014) considered variable operating pressures in their experiments for the removal of eight N-nitrosamine. For this purpose, the water permeability coefficient L_p and the friction parameter b will be estimated for each run from these experiments using the gEST parameter estimation tool available in the gPROMS (Process System Enterprise Ltd., 2001).

The estimation of these parameters is achieved by minimising the sum of the square errors (SSE) between the experimental outlet flow rate $F_{b(L)}$, total permeated water $F_{p(Total)}$, outlet feed pressure $P_{b(L)}$ and average N-nitrosamine rejection $Rej_{(av)}$ and the predicted values from the model.

The parameter estimation problem can be therefore described as follows:

Given: The time invariant parameters: Inlet feed concentration, flow rate, pressure and temperature.

The measured parameters: Outlet measured feed flow rate, pressure, water flux, total permeated flow rate, and average rejection.

Obtain: Water permeability coefficients and friction parameters.

Minimise: The sum of square errors (SSE).

Subject to: Process model, Process constraints.

SSE is defined as:

$$SSE = \sum_{i=1}^{N_{Data}} \left[F_{b(L),i}^{Exp.} - F_{b(L),i}^{Cal.}\right]^2 \tag{11}$$

Where N_{Data}, $F_{b(L)}^{Exp.}$ and $F_{b(L)}^{Cal.}$ are the numbers of test runs, experimental and the calculated retentate feed flow rate respectively. Also, it is important to mention that the estimation of friction factor (b) is mainly related to both the experimental and predicted value of the retentate pressure ($P_{b(L)}$) linked to the trans-membrane pressure drop along the module.

The parameter estimation problem can be mathematically presented as follows:

$$\min_{L_p,\, b} \quad SSE$$

Subject to:

Equality constraints:

Process Model: $f(z, x(z), x^{-}(z), u(z), v) = 0$; $[z_0, z_f]$

Inequality constraints:

$$L_p^{\,L} \leq L_p \leq L_p^{\,U}$$

$$b^L \leq b \leq b^{\,U}$$

L and U are the lower and upper bounds. The results of the parameter estimation are given in Table 2 which clearly show the variation of transport parameters with the inlet operating conditions for eight N-nitrosamine experiments. These results clearly establish the fact that a single model should not be blindly used under different conditions or for different pollutants but must be validated each time before it can be confidently used for simulation, design, optimisation, etc. For the convenience of the reader, few experimental and predicted values of retentate flow rate and retentate pressure are included in Table 3 with the calculation of relative error and sum of the squared errors. The results of parameter estimation (Table 2) show that permeability constants vary with the operating pressure enhancing (although slightly) the permeability constant of water with increasing pressure except for 10.1 atm that associated with higher values of friction.

The registered values of friction parameters vary between 58 to 353 atm s/m^4 for the operating pressures 4, 6.51 and 10.1 atm respectively. This in turn can confirm the relation between the operating pressure and friction factor. While, the parameter estimation method shows that the water permeability coefficients L_p for the set of used pressures varies between $1.0\text{x}10^{-6}$ to $1.30\text{x}10^{-6}$ m/s atm for the membrane type ESPA2-4040 Hydranautics, Oceanside, CA., USA at $2.43x10^{-3}$ m³/s and 20 °C of feed flow rate and temperature respectively. These model parameters were used for the remainder of this work. Table 4 includes the design and operating parameters of the spiral-wound membrane element.

Table 2. Results of parameter estimation

N-nitrosamine	$C_{s(0)}x10^9$ (kmol/m^3)	$P_{b(0)}$ (atm)	b (atm s/m^4)	$L_p x10^6$ (m/s atm)
NDMA	3.3761	4.0	58.89	1.1000
NDMA	3.3761	6.51	177.23	1.1293
NDMA	3.3761	10.1	352.74	1.1770
NMEA	2.8389	4.0	58.81	1.0878
NMEA	2.8389	6.51	177.76	1.1283
NMEA	2.8389	10.1	353.34	1.0730
NPYR	2.4985	4.0	59.46	1.0994
NPYR	2.4985	6.51	177.42	1.1349
NPYR	2.4985	10.1	351.14	1.0431
NDEA	2.4490	4.0	59.02	1.0000
NDEA	2.4490	6.51	176.24	1.3060
NDEA	2.4490	10.1	351.03	1.0053
NPIP	2.1914	4.0	58.96	1.0000
NPIP	2.1914	6.51	175.01	1.0565
NPIP	2.1914	10.1	352.53	1.0282
NMOR	2.1540	4.0	58.94	1.000
NMOR	2.1540	6.51	177.34	1.1724
NMOR	2.1540	10.1	353.15	1.0867
NDPA	1.9214	4.0	58.98	1.0000
NDPA	1.9214	6.51	177.64	1.0897
NDPA	1.9214	10.1	350.79	1.0568
NDBA	1.5808	4.0	58.96	1.0000
NDBA	1.5808	6.51	175.33	1.2104
NDBA	1.5808	10.1	351.86	1.0301

$F_{b(0)}$ = $2.43x10^{-3}$ m³/s and T_b = 20 °C

Table 3. Results of relative errors and sum of square errors

N-nitrosamine	$C_{s(0)}x10^9$ (kmol /m^3)	$P_{b(0)}$ (atm)	$F_{b(L)}^{Exp.}x10^3$ (m³/s)	$F_{b(L)}^{Cal.}x10^3$ (m³/s)	Relative Errors	$P_{b(L)}^{Exp.}$	$P_{b(L)}^{Cal.}$	Relative Errors	Sun of square errors *SSE* (-) $x10^4$

NDMA	3.3761	10.1	2.23	2.225	$4.31x10^{-6}$	7.890	7.895	$-5.28x10^{-3}$	5.16
NMEA	2.8389	10.1	2.23	2.234	$3.18x10^{-5}$	7.890	7.887	$1.09x10^{-2}$	9.44
NPYR	2.4985	10.1	2.23	2.233	$-3.35x10^{-6}$	7.890	7.893	$-3.71x10^{-3}$	3.69

Table 4. Specifications of the spiral-wound membrane element

Make	**Hydranautics, Oceanside, CA., USA**
Membrane type	ESPA2-4040
Module configuration	Spiral-wound
Membrane polymer	Composite Polyamide
Feed spacer thickness t_f (m)	$6.6x10^{-4}$
Membrane sheet active area (m^2)	7.9
Membrane sheet length L (m)	0.9
Membrane sheet width W (m)	8.7778
Characteristics length of spacer ΔL (m)	0.006
Membrane diameter (in) (m)	3.95, 0.1003
Maximum applied pressure (atm)	41.056
Maximum operating temperature (°C)	45
Salt Rejection (dimensionless)	99.6% (99.4 %minimum)

6. Model validation

The model data listed in Table A.1 in Appendix A has been validated by comparing the model predictions results with those obtained from actual experimentation of Fujioka et al. (2014) for a spiral-wound RO membrane. Fig. 3 compares the observed and modeled feed pressure along the x-axis of three membranes in series (2.7 m length) for three different overall permeate fluxes. Fig. 4 compares the observed and modeled average permeate flux and retentate flow rate as a function to inlet feed pressure. Finally, Fig. 5 compares the model rejections of eight N-nitrosamines solutes at three different overall permeate fluxes against experimental results, which shows high value of R^2. Furthermore, Fig. 4 shows that the model can be used to simulate the observed data of an outlet feed flow rate at high operating pressure (high average permeate flux) albeit with a minor deviation (1%). It is expected that the inaccurate estimation of the water permeability coefficient of such pressure might causes this deviation. It is important to note that Fujioka et al. (2014) have experimentally measured the feed pressure of each membrane (three in series) and plotted them against the total membranes length with a fitting line. While, the model developed by Al-Obaidi et al. (2017b) can estimate the pressure at any dimension of x-axis (one dimensional distributed model).

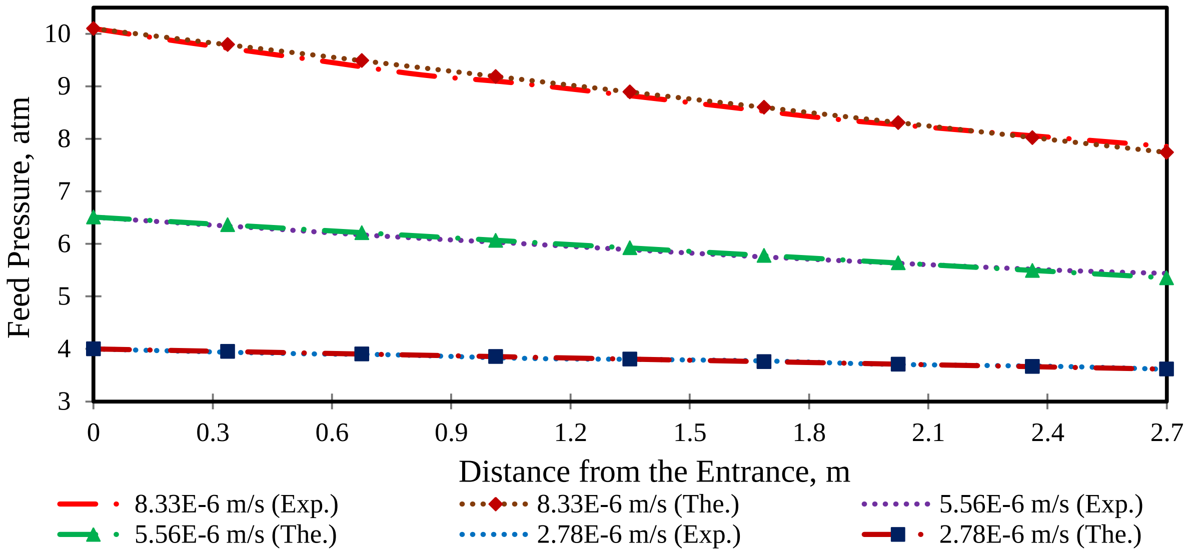

Fig. 3. Observed and modeled feed pressure versus the membrane length for three different average permeate fluxes (initial conditions of NDMA, 3.3761×10^{-9} kmol/m³, 2.43×10^{-3} m³/s and 20 °C)

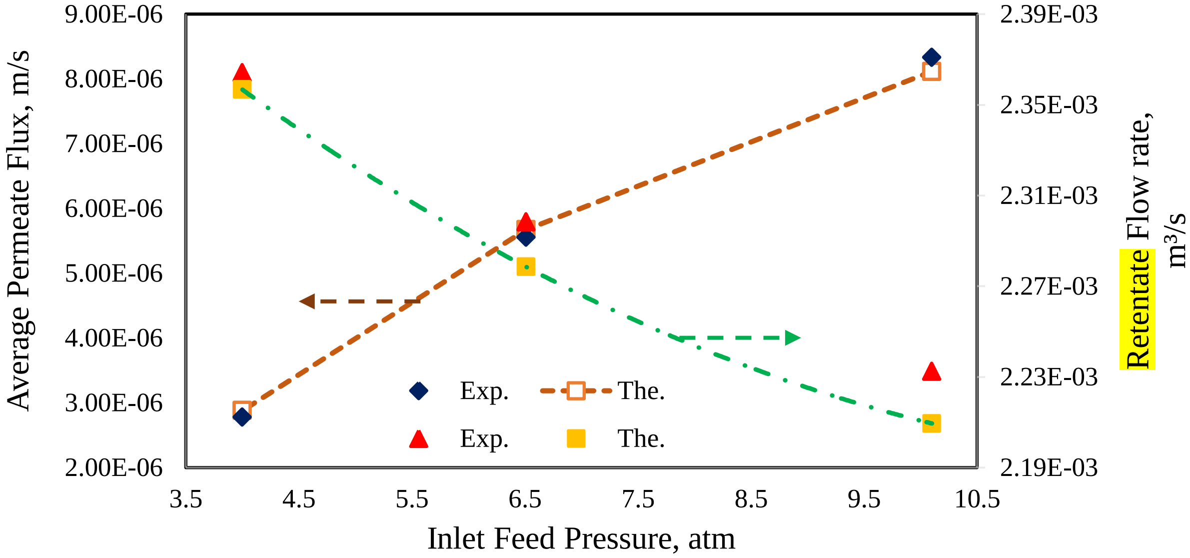

Fig. 4. Observed and modeled average permeate flux and retentate flow rate versus inlet feed pressure (initial conditions of NDMA, 3.3761×10^{-9} kmol/m³, 2.43×10^{-3} m³/s and 20 °C)

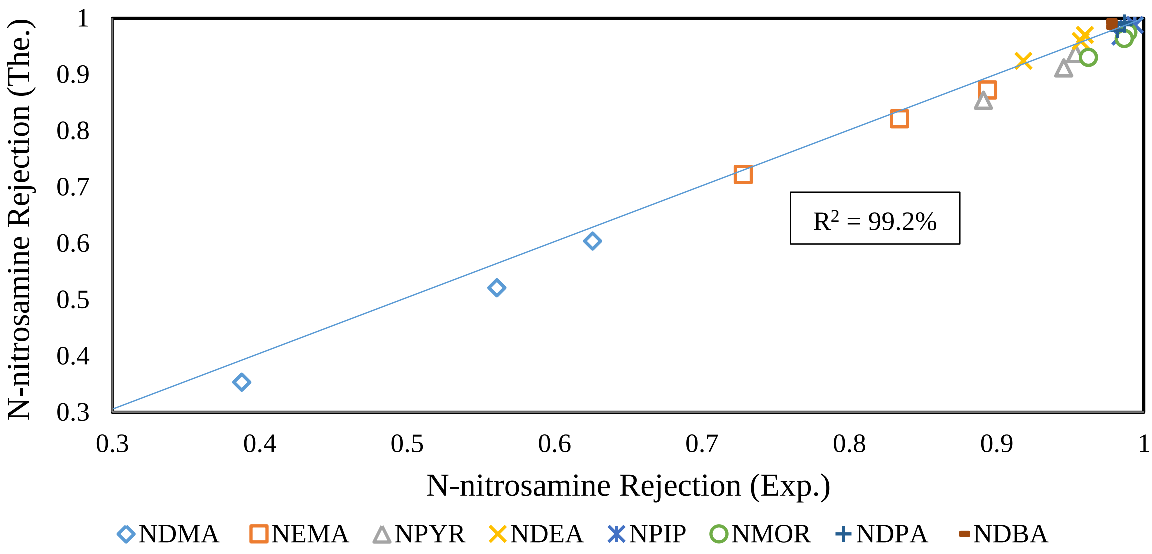

Fig. 5. Experimental and modelled rejections of eight N-nitrosamine solutes at three average permeate fluxes of (2.78×10^{-6}, 5.56×10^{-6} and 8.33×10^{-6} m/s) (initial conditions, 2.43×10^{-3} m³/s and 20 °C)

7. Process Simulation: Effect of operating parameters

To have a better insight of the impact of operating parameters on several performance measures of the process (such as N-nitrosamine rejections, specific energy consumptions, etc.), simulations of the process configurations (Fig.1 and Fig. 2) are carried out before optimization formulation and results are presented.

7.1 *Effect of inlet feed pressure*

Table 2 shows that the friction parameter increases due to an increase in the operating feed pressure. Fig. 6 shows a linear relationship between the applied feed pressure and friction factor for a spiral-wound RO module type ESPA2-4040. This relation will be used to estimate the friction parameter for each run of operating pressure.

The solute rejection, total recovery and specific energy consumption are directly affected by the operating feed pressure of the RO filtration system, which directly affects the solvent and solute fluxes through the membrane (Thomson et al., 2002). The impact of inlet feed pressure variation at constant inlet feed flow rate and temperature of 2.43E-3 m³/s and 20 ºC respectively on N-nitrosamine rejection, total recovery, and specific energy consumption for the RO configurations (shown in Fig.1 and Fig. 2) is highlighted within the manufacturer's specification of membrane area and the maximum operating pressure.

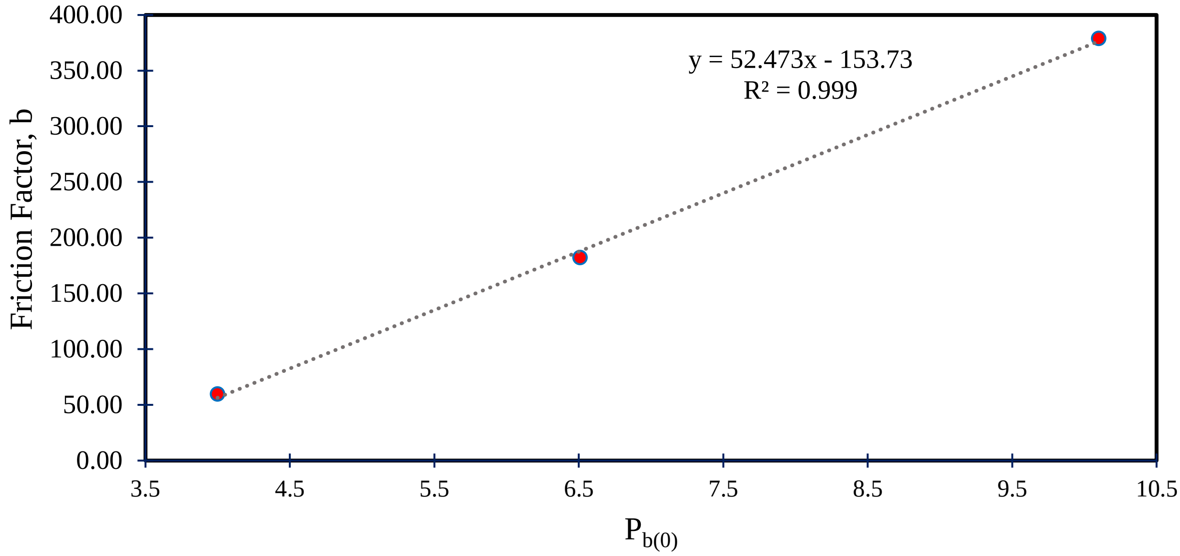

Fig. 6. Friction parameter versus inlet feed pressure for module type ESPA2-4040 (with initial conditions, 2.43×10^{-3} m^3/s and 20 °C)

Fig. 7 displays the relationship existing between the inlet feed pressure and N-nitrosamine rejection for three different compounds using their initial concentrations as presented in Table 2. It is clearly shown that increasing the feed pressure from 10.1 to 40 atm (within the manufacturer's specification, Table 3) has a significant impact on N-nitrosamine rejection. It is expected that higher permeate flux increases the dilution of solute at the feed side, which passed through the membrane, and therefore results in lower permeate concentration. NDMA rejection is increased by 30% from 0.60 to 0.78 as a response to an increase in the inlet feed pressure from 10.1 to 40 atm. NMEA and NPYR rejections are increased simultaneously by 9.57% and 4.55% from 0.87 to 0.95 and from 0.936 to 0.978 respectively. These results indicate that the higher feed pressure is required to obtain higher N-nitrosamine rejection due to an increase in water flux and total water recovery.

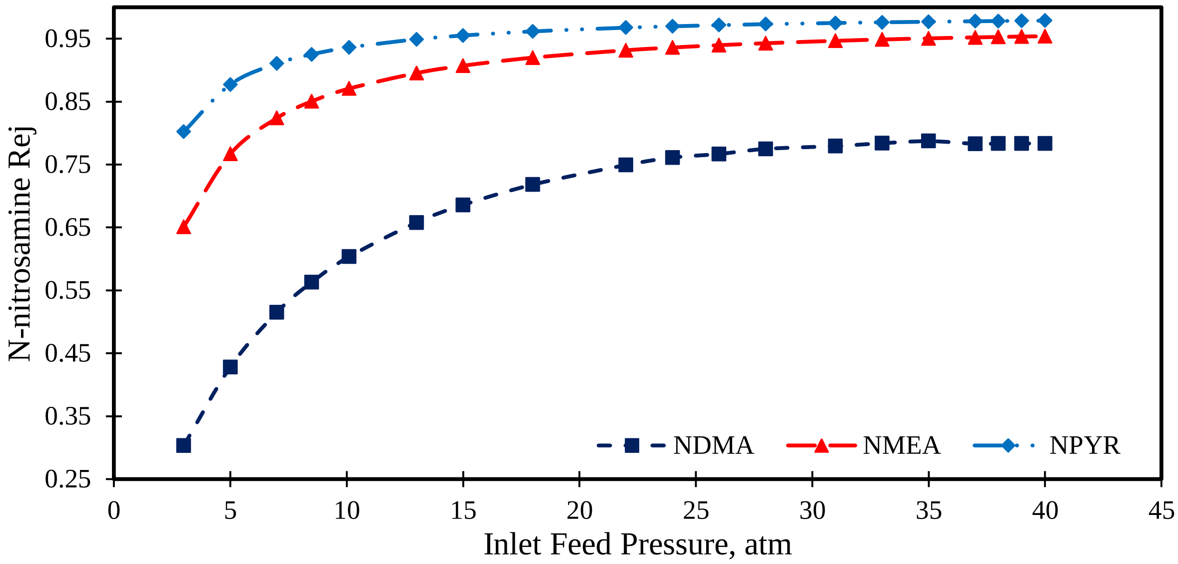

Fig. 7. Dependence of N-nitrosamine rejection on inlet feed pressure at inlet feed conditions of 2.43×10^{-3} m³/s and 20 °C

Fig. 8 displays the relationship existing between the specific energy consumption and total recovery as a function of inlet feed pressure for the RO configurations (Figs. 1 and 2). This includes an investigation of the impact of both HPP and ERD efficiency for the same step change in inlet feed pressure. It is clear that the energy consumption decreases with increasing inlet feed pressure in case of using only HPP. This lower energy consumption is caused by an increase in the efficiency of pump from 80% to 85% and then to 90%. More specifically, the energy consumption is brought down by a constant value of 5.88 % for all pressures by increasing the pump efficiency from 80% to 85%, while, a reduction of a constant value of 5.55% for all pressures is registered by increasing the pump efficiency from 85% to 90%. Therefore, using a higher efficiency pump can significantly reduce the energy consumption. These results concur with the findings of Du et al. (2014).

For the RO system shown in Fig. 2, Fig. 8 shows that the addition of ERD in the RO filtration system is very important where the energy consumption can be reduced by approximately 47% at operating pressure of 10.1 atm and 31% at 40 atm than the case of only HPP mode. The reason for this is that the rejected stream flow rate is about 61 – 97% of the inlet feed flow rate and the outlet brine pressure is about 74 – 99% of the inlet pressure for a set of operating pressure varied between 40 to 3 atm, which results in a high amount of hydraulic energy in the rejected side. This is a substantial energy saving for the system. Also, these results indicate that increasing feed pressure will increase the total water recovery as well as an increase in the specific energy consumption. The impact of increasing the efficiency of

ERD is shown by reducing the consumption of energy. However, it is clearly shown that the impact of pressure on energy consumption is more obvious at low pressures than at high pressures. The consumption of energy is slightly increased at high recovery region in comparison to a dramatic growth at low recovery region (low operating pressures). The reason of this phenomenon is that at high feed pressures and recoveries, the quantity of water to be pressurised will be less than at low recoveries and pressures. Another explanation can be drawn from Fig. 9 which shows a steady increase of the pressure difference between the inlet and outlet pressures due to an increase in inlet pressure. This shows that higher recovery can be achieved at higher pressures due to a higher-pressure difference along the membrane length, which reduces the energy consumption for HPP mode as illustrated in Eq. (5) in comparison to lower operating pressures, which are characterised by lower values of pressure difference and higher energy consumption. However, Fig. 8 shows that the energy consumption increases due to an increase in water recovery for the system. This test indicates that the beneficial effect of ERD addition becomes less significant in energy saving at high operating pressures in comparison to low operating pressures despite achieving higher solute rejection and lower energy consumption when compared with HPP mode.

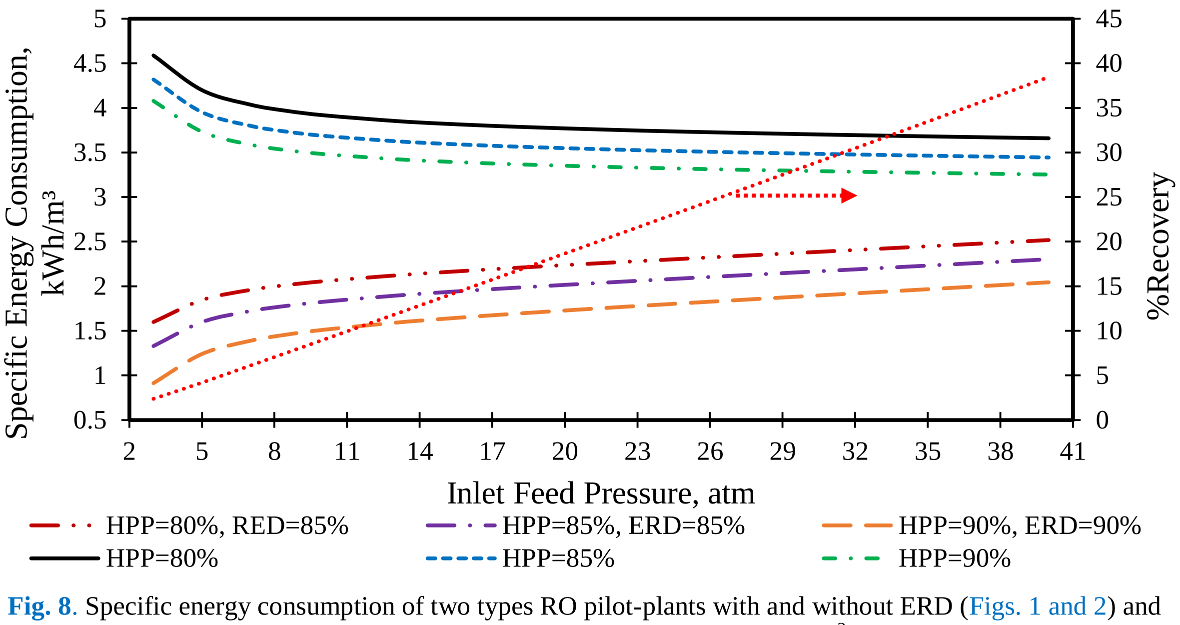

Fig. 8. Specific energy consumption of two types RO pilot-plants with and without ERD (Figs. 1 and 2) and total recovery versus inlet feed pressure at inlet feed conditions of 2.43×10^{-3} m³/s and 20 °C (Note: The efficiency of booster pump is assumed same as high pressure pump)

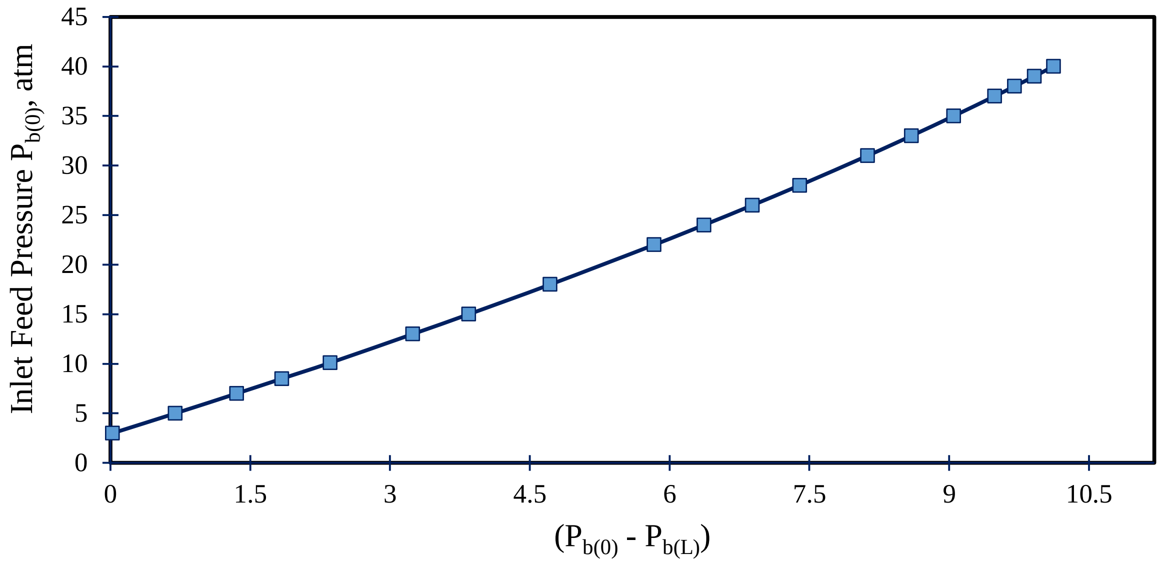

Fig. 9. The relation between the inlet feed pressure and the pressure difference at inlet and outlet edges at inlet conditions of 2.43 x10^{-3} m³/s and 20 °C

7.2 Effect of inlet feed flow rate

The influence of the inlet feed flow rate at constant values of inlet feed pressure and temperature on N-nitrosamine rejection and energy consumption is considered in this section. The inlet feed flow rate is reduced by 50% from 2.43x10^{-3} m³/s to 1.215x10^{-3} m³/s by 10% step change for each run at constant inlet feed pressure and temperature of 10.1 atm and 20 ºC respectively.

It was found that a maximum recovery can be achieved at low inlet feed flow rate. This behaviour is due to the pressure drop in the high-pressure channel, which decreases when the operating feed flow rate also decreases. Similarly, an increase in the feed flow rate will increase the loss in pressure due to higher friction along the membrane length. This reduces the advantage of having a lower average osmotic pressure and concentration polarisation; as this in turn decreases the water flux and total permeate recovery. It can therefore be concluded that N-nitrosamine rejection insignificantly decreases due to increase in the feed flow rate as can be shown in Fig. 10. These results are in line with the findings of Abbas (2005).

Moreover, increasing the inlet feed flow rate at constant pressure and temperature will increase the specific energy consumption due to a lower gain in total recovery, as can be shown in Fig. 11. Therefore, at constant operating pressure and temperature, it is recommended to work within low feed flow rates to guarantee lower energy consumption and higher solute rejection.

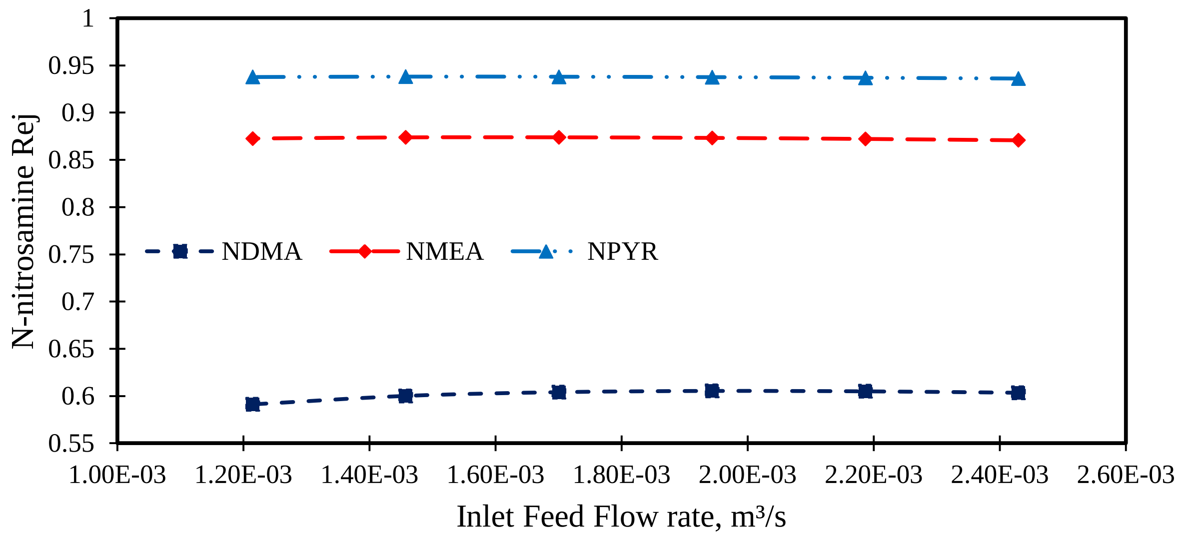

Fig. 10. Dependence of N-nitrosamine rejection on inlet feed flow rate at inlet feed conditions of 10.1 atm and 20 °C

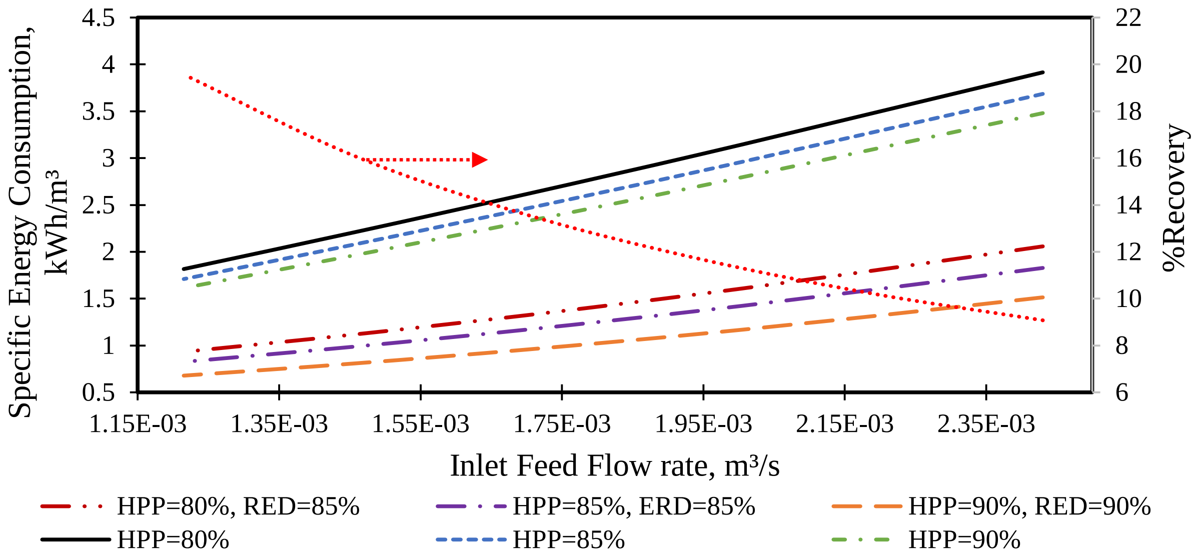

Fig. 11. Specific energy consumption of two types RO pilot-plants with and without ERD and total recovery versus inlet feed flow rate at inlet feed conditions of 10.1 atm and 20 °C

7.3 Effect of inlet feed temperature

The inlet feed temperature can have a clear effect on solute rejection, water recovery and energy consumption according to Jiang et al. (2015). In this work, we evaluated and reported the performance of the RO network for every 2 ºC rise in feed temperature (note the reference feed temperature is 20 ºC). The total permeate recovery increase due to an increase in the feed temperature at constant inlet feed flow rate and pressure (Figs. 12 and 13). This is compared to a slight decrease of N-nitrosamine compounds rejection. This same trend has been reported by Fujioka (2014) which is already attributed to increase the membrane pore size as a result to increasing operating temperature in addition to increasing the solute transport parameter. This in turn increases the solute flux and reduces the rejection parameter. The registered reduction of NDMA, NEMA and NPYR rejections are 6.5%, 1.7%, and 0.79% respectively, compared to 67% increase in total recovery rate, when the temperature gradually increases from 20 to 44 °C. More specifically, the rejections are decreased from 0.6 to 0.56 for NDMA and from 0.87 to 0.85 for NEMA and from 0.936 to 0.926 for NPYR (Fig. 12). Occasionally, the gain of energy consumption is around 28% and 32% for with and without ERD configurations (Fig. 13). These results show the significant role of feed temperature to capture higher recovery rate in addition to lower energy consumptions.

However, the above results did not include the contribution of the boiler energy required to raise the feed temperature from 20 to 44 ºC. We assumed 1 hour to raise the feed temperature to the next level and the total heat supplied, Q, in Watt, is calculated using Eq. (7) with assuming no heat loss. To be consistent with Eqs. (4) and (5), the heat supplied is divided by the volume of produced permeate in Eq. (8) to calculate the boiler energy consumption. Eq. (9) then gives the total energy consumption for the whole system.

Fig. 13 also shows the cases of the total energy consumption of the system. As expected, the addition of this energy will lift the total energy consumption of the whole system. However, the interesting point here is that the consumption of energy with the boiler addition is still lower than the registered values of RO consumption without the ERD mode. Also, Fig. 13 shows that the total energy consumption of the process (Fig. 2) is reasonably increased from 20 to 22 °C due to the addition of consumed boiler power calculated by Eq. (8) and then continuously decreased when the tank temperature increased from 22 to 44 ºC. This can be explained due to a noticeable increase of permeate flowrate as a result of increasing feed temperature. The increasing total permeate $(F_{p(Total)})$ will reduce the total energy consumptions (E1, E2, E3, E4) according to Eqs. (4), (5), (8) and (9). Note that the calculation of the boiler energy consumption is carried out when the temperature increases by an increment of 2 °C assuming no heat loss. This is done by assuming that wastewater will keep its energy before supplying any further heat.

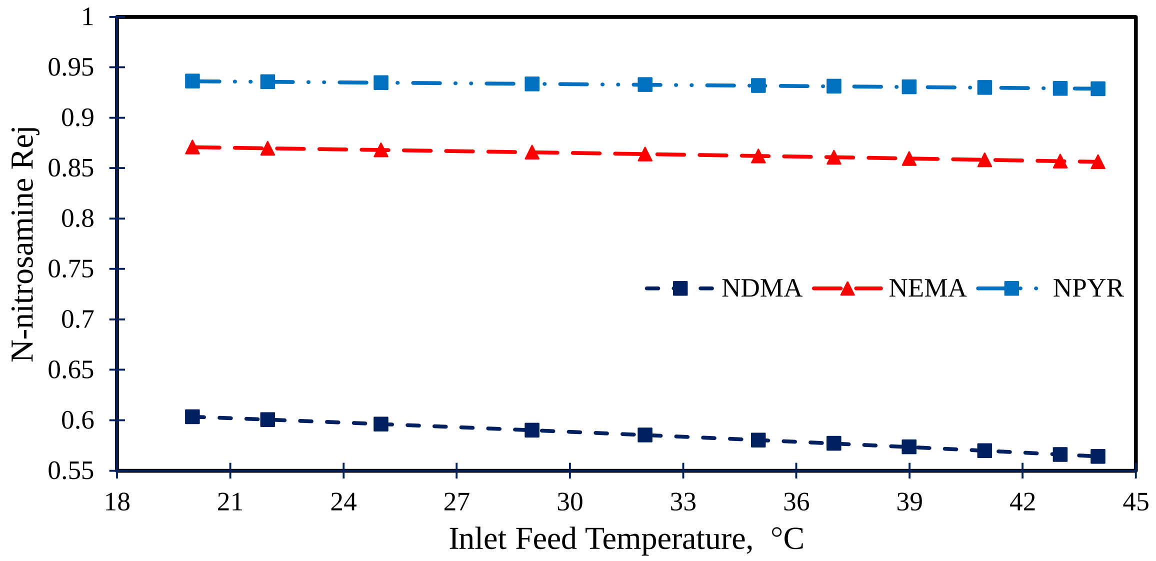

Fig. 12. Dependence of N-nitrosamine rejection on inlet feed temperature at inlet feed conditions of 2.43x10^{-3} m³/s and 10.1 atm

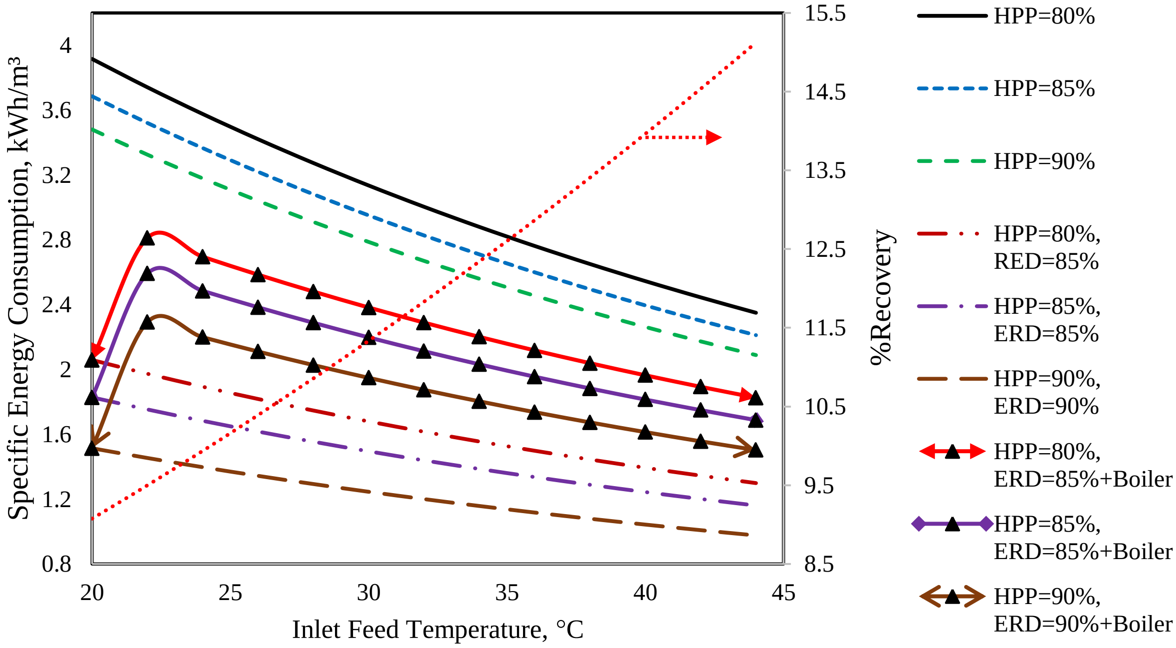

Fig. 13. Specific energy consumption of two types RO pilot-plants with and without ERD and ERD with Boiler and total recovery versus inlet feed temperature at inlet conditions of 2.43x10^{-3} m/s and 10.1 atm

Finally, it is easy to notice that an increase in the inlet feed pressure (at a constant feed flow rate and temperature) has a significant impact on N-nitrosamine rejection and total recovery. This is compared to a negative impact on N-nitrosamine rejection due to increasing the operating temperature (at constant pressure and flow rate), and flow rate (at a constant pressure and temperature). However, it is evident that the increment in the inlet feed flow rate has a negative impact on total permeate recovery. Moreover, both an increase in the inlet feed pressure (at a constant feed flow rate and temperature) and feed flow rate (at a constant feed pressure and temperature) have an adverse impact on energy consumption of ERD and HPP configurations. Also, an increase in the inlet feed temperature (at constant feed pressure and flow rate) will increase the consumption of energy within acceptable levels despite the added consumed energy of the boiler (source of heat). Also, the combination of ERD and HPP (Fig. 2) can lead to a higher reduction in energy consumption compared to the experimental RO pilot-plant used by Fujioka et al. (2014) (Fig. 1).

8. Process Optimisation

Having developed a deeper insight (in the earlier sections) of the impact of a number of operating parameters (by varying these parameters one at a time) on the rejection rates of N-nitrosamine contaminants and energy consumptions for two given RO configurations with and without energy recovery options (Fig. 1 and Fig. 2), we have decided to formulate two optimisation problems which will maximize the rejection rates and minimise the energy consumptions while optimizing the operating parameters. The readers are directed to the work of Evangelista et al. (1985), El-Halwagi (1992), Voros et al. (1997), Maskan et al, (2000), Marriott et al. (2003), Guria et al. (2005), Marcovecchio et al. (2005), and Lu et al. (2007) to have further exposure to different optimisation techniques applied in membrane-based separation processes including RO,

The first objective is to maximise the NDMA rejection of the configuration of RO pilot-plant used by Fujioka et al. (2014) (Fig. 1, without ERD) and the RO system described in Fig. 2 by allowing the system operating conditions to vary within the limits set in the manufacturer's specification. Any optimised operating conditions that maximise NDMA rejection would serve the rejections of NMEA and NPYR too.

The second objective is to minimise the total energy consumption of the two configurations (Fig. 1 and Fig. 2) measured in kWh per m^3 of the total permeate. The results of Fujioka et al. (2014) for solute rejections were taken as the minimum accepted values for the optimisation.

8.1 Optimisation Problem 1 (OP1)

The optimisation problem can be described as follows:

Given: Operating feed conditions, module specifications.

Optimise: Inlet feed pressure, flow rate and temperature (the optimisation variables).

Maximize: NDMA rejection.

Subject to: Equality (process model) and inequality constraints (linear bounds of optimisation variables).

As the optimisation problem can be represented mathematically as:

OP1:

$$\max_{F_{b(0)}, P_{b(0)}, T_b} \quad Rej$$

Subject to:

Equality constraints:

Process Model: $f(z, x(z), \bar{x}(z), u(z), v) = 0; \quad [z_0, z_f]$

Inequality constraints:

$$(1\text{x}10^{-3}\ m^3/s) \quad {F_{b(0)}}^L \leq F_{b(0)} \leq {F_{b(0)}}^U \quad (2.43\text{x}10^{-3}\ m^3/s)$$

$$(3.0\ atm) \quad {P_{b(0)}}^L \leq P_{b(0)} \leq {P_{b(0)}}^U \quad (41.0\ atm)$$

$$(20\ ^{o}C) \quad T_b^L \leq T_b \leq T_b^U \quad (44\ ^{o}C)$$

The optimisation will be carried out for only NDMA, NMEA and NPYR with initial feed concentrations shown in Table 1.

8.2 Optimisation Problem 2 (OP2):

The optimisation problem can be described as follows:

Given: Operating feed conditions, module specifications.

Optimise: Inlet feed pressure, flow rate and temperature (the optimisation variables).

Minimise: The specific energy consumption defined in Eq. (9).

Subject to: Equality (process model) and inequality constraints (linear bounds of optimisation Variables and solute rejection)

As the optimisation problem can be represented mathematically as:

$$\underset{F_{b(0)}, P_{b(0)}, T_b}{\text{Min}} \quad E_4 \text{ (defined in Eq. 9)}$$

Subject to:

Equality constraints:

Process Model: $f(z, x(z), x^{-}(z), u(z), v) = 0; \quad [z_0, z_f]$

Inequality constraints:

$$(1\text{x}10^{-3}\ m^3/s)\ \ {F_{b(0)}}^L \leq F_{b(0)} \leq {F_{b(0)}}^U\ \ (2.43\text{x}10^{-3}\ m^3/s)$$

$$(3.0\ atm)\ \ {P_{b(0)}}^L \leq P_{b(0)} \leq {P_{b(0)}}^U\ \ (41.0\ atm)$$

$$(20\ ^{\circ}C)\ \ T_b^L \leq T_b \leq T_b^U\ \ (44\ ^{\circ}C)$$

$$Rej_{NDMA} \geq 0.6273 \quad Rej_{NMEA} \geq 0.8864 \quad Rej_{NPYR} \geq 0.9454$$

Firstly, the results of Fujioka et al. (2014) are given in the first row of Table 5 for the purpose of comparison with the optimisation results (base case). For OP1, the maximum rejections for NDMA, NMEA and NPYR are found to be 0.80, 0.951 and 0.977 with optimum feed flowrate of $2.43\text{x}10^{-3}$ m^3/s, pressure 35.406 atm and temperature at 20 °C with significant reduction (4.48 kWh/m^3 to 3.678 kWh/m^3 to 2.454 kWh/m^3) in energy consumption (for all energy recovery options). For NDMA, NMEA and NPYR there is an increase of 27.5%, 7.3% and 3.34% in rejections respectively compared to Fujioka et al. (2014). Interestingly, the optimisation confirms that the RO process is not efficient for the removal of NDMA (compared to NMEA and NPYR) as reported by Mitch et al. (2003).

Increasing the operating temperature from 42 ºC to 44 °C at the optimised conditions of OP1 showed a positive impact on the reduction in energy consumptions (all options) compared to the case at 20 °C. However, NDMA, NMMA and NPYR rejections are decreased to 0.514, 0.915 and 0.962 respectively.

The results of OP2 show that the minimum energy consumption can be significantly reduced from 4.48 kWh/m^3 to 1.912 kWh/m^3 to 1.046 kWh/m^3 with no significant gain of N-nitrosamine rejection compared to the base case. This was possible for a much lower value of feed rate ($1.30\text{x}10^{-3}$ m^3/s), pressure (12.98 atm), and temperature at 20 °C compared to Fujioka et al. (2014). The reduction of specific energy consumption was about 57.3% compared to Fujioka et al. (2014).

Increasing the operating temperature from 42 ºC to 44 °C, OP2 results in further reduction in energy consumption (1.146 and 0.73 kWh/m³ for Figs. 1 and 2 respectively) with the same optimized conditions of OP2. For this case, the NDMA, NMEA and NPYR rejections are found to be 0.514, 0.866 and 0.936 respectively which are worse than those found at 20 °C. The reduction of specific energy consumption was about 74.4% compared to Fujioka et al. (2014). The results in Table 5 clearly indicate how the inlet feed pressure, temperature, and feed flow rate can potentially affect N-nitrosamine rejection and plays an important role in reducing the energy consumption.

Table 5. The optimisation results

No.	Optimisation Problem	$F_{b(0)}$x 10^3,m³/s	$P_{b(0)}$, atm	T_b, °C	*Rej* (NDMA)	*Rej* (NMEA)	*Rej* (NPYR)	Energy Consumption kWh/m³ HPP 80% (Fig. 1)	HPP 80%+ERD 85%	Boiler Consumed Power	(total energy consumption) HPP 80%+ERD 85%+Boiler (Fig. 2)	Comments
1	Base Case	2.43	10.100	20	0.6273	0.8864	0.9454	4.48	0	0	4.48	Fujioka et al. (2014) results
2	OP1	2.43 (opt)	35.406 (opt)	20 (opt)	0.80 (max)	0.951 (max)	0.977 (max)	3.678 (calc)	2.454 (calc)	0	2.454 (calc)	Optimised rejection at 20 °C
3	OP1	2.43 (opt)	35.406 (opt)	42-44 (Selected)	0.514	0.915	0.962	2.181 (min)	1.686 (min)	0.139	1.825	Calculated energy consumption at 44 °C
4	OP2	1.30 (opt)	12.982 (opt)	20 (opt)	0.634 (calc)	0.8941 (calc)	0.949 (calc)	1.912 (min)	1.046 (min)	0	1.046	Optimised energy consumption at 20 °C
5	OP2	1.30 (opt)	12.982 (opt)	42-44 (Selected)	0.514 (calc)	0.866 (calc)	0.936 (calc)	1.146 (min)	0.730 (min)	0.374	1.104	Calculated energy consumption at 44 °C

Inlet feed concentration $C_{b(0)}$ of each N-nitrosamine is given in Table 1. opt = optimised value; max = maximised value; min = minimised value

9. Conclusions

In this work, the removal of N-nitrosamine compounds from wastewater is considered using an experimental RO process considered in the literature (Fig. 1). The impact of different operating parameters such as inlet feed pressure, flow rate and temperature on the rejection of N-nitrosamine compounds is investigated in detail using modelling and simulation. The process model used for this purposed has been validated using experimental data from the literature which in turn estimated a number of model parameters. A number of energy recovery options have also been considered on the process (Fig. 2) and the impact of different operating parameters on the energy consumption is evaluated.

Having developed clear understandings of the impact of a number of operating parameters on the rejection of N-nitrosamine compounds and the energy consumption via sensitivity analysis (varying one parameter at a time), it was decided to simultaneously optimise these parameters to either maximise the rejections or minimise the energy consumption of the process. The optimisation results clearly show that rejection of some of the compounds can be improved by more than 27% and energy consumption can be minimised by more than 70%. Specifically, NDMA rejection is improved from 62.7% to 80%. Also, the energy consumption is improved from 4.48 to 1.1 kWh/m^3 at the optimised operating conditions.

Symbols

b : The feed channel friction parameter (atm s/m^4)

B_s : The solute permeability coefficient used in the Solution-diffusion model (m/s)

$C_{\tilde{s}(av)}$: The average mean solute concentration in the feed channel (kmol/m^3)

$C_{\tilde{s}(0)}$: The inlet mean solute concentration (kmol/m^3)

$C_{\tilde{s}(L)}$: The outlet mean solute concentration (kmol/m^3)

$C_{p(av)}$: The average permeate solute concentration in the permeate channel (kmol/m^3)

C_p : The specific heat capacity of water (4181 j/kg K)

$C_{s(0)}$: The inlet feed solute concentrations in feed channel (kmol/m^3)

$C_{s(L)}$: The outlet feed solute concentrations in feed channel (kmol/m^3)

$C_{w(x)}$: The molar solute concentration on the membrane surface at any point along the x-axis in feed channel (kmol/m^3)

$D_{b(x)}$: The solute diffusion coefficient of feed at any point along the x-axis (m^2/s)

$E1$: The specific energy consumption for high pressure pump (kW h/m^3)

$E2$: The specific energy consumption for high pressure pump and ERD (kW h/m³)

$E3$: The specific energy consumption for the boiler (kW h/m³)

$E4$: The specific energy consumption for high pressure pump, ERD and Boiler (kW h/m³)

ERD : Energy recovery device

$F_{b(x)}$: The feed flow rate at any point along the x-axis in feed channel (m³/s)

$F_{b(0)}$: The feed flow rate at x=0 in feed channel (m³/s)

$F_{b(L)}$: The feed flow rate at x=L in feed channel (m³/s)

$F_{b(ERD)}$: The feed flow rate of energy recovery device (m³/s)

$F_{b(HPP)}$: The feed flow of the high pressure pump (m³/s)

$F_{b(Tank)}$: The feed flow rate of feed tank (m³/s)

$F_{p(x)}$: The permeate flow rate at any point along the x-axis in permeate channel (m³/s)

$F_{p(Total)}$: The total permeated flow rate at the permeate channel (m³/s)

$F_{in(Tank)}$: The inlet feed flow rate to the feed tank (m³/s)

$F_{out(Tank)}$: The outlet feed flow rate from the feed tank (m³/s)

HPP : High pressure pump

$J_{s(x)}$: The solute molar flux through the membrane at any point along the x-axis (kmol/m² s)

$J_{w(x)}$: The water flux at any point along the x-axis (m/s)

K: The efficiency of mixing net (i.e. spacer) (K = 0.5) (dimensionless)

$k_{(x)}$: The mass transfer coefficient at any point along the x-axis (m/s)

L : The length of the membrane (m)

L_p : The solvent transport coefficient (m/atm s)

$P_{b(x)}$: The feed channel pressure at any point along the x-axis (atm)

P_p : The permeate channel pressure (atm)

P_{atm} : The pressure of feed tank (1 atm)

$P_{b(ERD)}$: The outlet pressure of energy recovery device (atm)

R : The gas low constant (R=0.082 atm m³/ K kmol)

Rej : The solute rejection coefficient (dimensionless)

Q : The supplied heat by the boiler (j/s)

T_b : The feed temperature (°C)

T_{Ref} : The reference temperature (ºK)

T_{Tank} : The temperature accumulated at the tank (ºK)

t_f : The feed spacer thickness (m)

$U_{b(x)}$: The feed velocity at any point along x-axis in feed channel (m/s)

V : The volume of feed tank (m^3)

W : The membrane width (m)

x : The specific width of the membrane (m)

Z : Parameter defined in Eq. (2) in Table A.1 in Appendix A

Subscript

$\rho_{b(x)}$: The feed density at any point along the x-axis in feed channel (kg/m^3)

σ : The reflection coefficient (dimensionless)

ρ : The density of water (1000 kg/m^3)

ω : The solute permeability coefficients of the membrane ($kmol/m^2$ s atm)

ΔL : The characteristics length of spacer (m)

Δx : Length of the sub-section (m)

$\Delta P_{b(x)}$: Trans-membrane pressure at any point along the x-axis (atm)

$\Delta \pi_{s(x)}$: The osmotic pressure difference at any point along the x-axis (atm)

$\mu_{b(x)}$: The Feed viscosity at any point along the x-axis (kg/m s)

ε_{pump} : Pump efficiency (dimensionless)

ε_{ERD} : Energy recovery device efficiency (dimensionless)

ε_{BP} : Booster pump efficiency (dimensionless)

β : The leakage ration of ERD (dimensionless)

References

Abbas, A.,2005. Simulation and analysis of an industrial water desalination plant. Chemical Engineering and Processing, 44, 999–1004.

Akin, O., Temelli, F., 2011. Probing the hydrophobicity of commercial reverse osmosis membranes produced by interfacial polymerization using contact angle, XPS, FTIR, FE-SEM and AFM. Desalination, 278, 387–396.

Al-Obaidi, M., Li, J-P., Kara-Zaitri, C., Mujtaba, I.M., 2017a. Optimisation of reverse osmosis based wastewater treatment system for the removal of cholorophenol using Genetic Algorithm. Chemical Engineering Journal, 316, 91–100.

Al-Obaidi, M., Kara-Zaitri, C., Mujtaba, I.M., 2017b. Modeling of a spiral-wound reverse osmosis process and parameter estimation. Desalination and Water Treatment, 69, 93–101.

Anderson, W., Stover, R., Martin, J., 2009. Keys to high efficiency, reliable performance and successful operation of SWRO processes. In IDA World Congress, Dubai, UAE.

Bond, T., Huang, J., Templeton, M.R., Graham, N., 2011. Occurrence and control of nitrogenous disinfection by-products in drinking water – a review. Water Research, 45, 4341–4354.

Butt, F.H., Rahman F., Baduruthamal U., 1997. Hollow fine fiber vs. spiral-wound reverse osmosis desalination membranes Part 2: Membrane autopsy. Desalination, 109, 83-94

Du, Y., Xie, L., Liu, J., Wang, Y., Xu, Y., Wang, S., 2014. Multi-objective optimisation of reverse osmosis networks by lexicographic optimisation and augmented epsilon constraint method. Desalination, 333, 66–81.

El-Halwagi, M., 1992. Synthesis of reverse osmosis networks for waste reduction, AIChE J., 38(8), 1185–1198.

Evangelista, F., 1985. A Short-cut, Method for the design of reverse – osmosis desalination plants. Ind. Eng. Chem. Process Des., 24(1) 211–223.

Fujioka, T., 2014. Assessment and optimisation of N-nitrosamine rejection by reverse osmosis for planned potable water recycling applications. PhD Thesis, University of Wollongong.

Fujioka, T., Khan, S.J., Mcdonald, J.A., Roux, A., Poussade, Y., Drewes, J.E., Nghiem, L.D., 2014. Modelling the rejection of N-nitrosamines by a spiral-wound reverse osmosis system: Mathematical model development and validation. Journal of Membrane Science, 454, 212–219.

Geraldes, V., Pereira, N.E., de Pinho, M.N., 2005. Simulation and optimisation of medium-sized seawater reverse osmosis processes with spiral-wound modules. Industrial and Engineering Chemistry Research, 44, 1897–1905.

Greenlee, L.F., Lawler, D.F., Freeman, B.D., Marrot, B., Moulin, P., 2009. Reverse osmosis desalination: water sources, technology, and today’s challenges. Water Research, 43, 2317–2348.

Guria, C., Prashant, K., Bhattachary, S., Gupta, S.K., 2005. Multi-objective optimization of reverse osmosis desalination units using different adaptations of the non-dominated sorting genetic algorithm (NSGA). Comput. Chem. Eng., 29, 1977–1995.

Jiang, A., Wang, J., Biegler, L.T., Cheng, W., Xing, C., Jiang, Z., 2015. Operational cost optimisation of a full-scale SWRO system under multi-parameter variable conditions. Desalination, 355,124–140.

Koroneos, C., Dompros, A., Roumbas, G., 2007. Renewable energy driven desalination systems modelling. J. Clean. Prod., 15, 449–464.

Krauss, M., Longrée, P., van Houtte, E., Cauwenberghs, J., Hollender, J., 2010. Assessing the Fate of Nitrosamine Precursors in Wastewater Treatment by Physicochemical Fractionation. Environmental Science and Technology, 44 (20), 7871–7877.

Lu, Y., Hua, Y.D., Zhang, X.L., Wu, L.Y., Liu, Q.Z., 2007. Optimum design of reverse osmosis system under different feed concentration and product specification, J. Membr. Sci., 287(1), 219–219.

Madaeni, S.S., Koocheki, S., 2006. Application of taguchi method in the optimisation of wastewater treatment using spiral-wound reverse osmosis element. Chemical Engineering Journal, 119, 37–44.

Marcovecchio, M.G., Aguirre, P.A., Scenna, N.J., 2005. Global optimal design of reverse osmosis networks for seawater desalination: modeling and algorithm. Desalination, 184, 259–271.

Marriott J., Sorensen E., 2003. The optimal design of membrane systems, Chem. Eng. Sci., 58(1), 4991–5004.

Maskan, F., Wiley, D.E., Johnston, P. M., 2000. Optimal design of reverse osmosis module networks. AIChE J., 46(5), 946–954.

Mitch, W. A., Sharp, J. O., Trussell, R. R., Valentine, R. L., Alvarez-Cohen, L., Sedlak, D. L., 2003. N-nitrosodimethylamine (NDMA) as a drinking water contaminant: A review. Environ. Eng. Sci., 20, 389–404.

Miyashita, Y., Park Sang-Hyuck, Hyung H., Huang Ching-Hua, Kim Jae-Hong., 2009. Removal of N-Nitrosamines and Their Precursors by Nanofiltration and Reverse Osmosis Membranes. Journal of Environmental Engineering, 788–795.

Murthy, Z.V.P., Gupta, S.K., 1999. Sodium cyanide separation and parameter estimation for reverse osmosis thin film composite polyamide membrane. Journal of Membrane Science, 15, 89–103.

Oh, H., Hwang, T., Lee, S., 2009. A simplified simulation model of RO systems for seawater desalination. Desalination, 238, 128–139.

Process System Enterprise Ltd., 2001. gPROMS Introductory User Guide. London: Process System Enterprise Ltd.

Qi, B., Wang, Y., Xu, S., Wang, Z., Wang, S., 2012. Operating energy consumption analysis of RO desalting system: Effect of membrane process and energy recovery device (ERD) performance variables. Industrial and Engineering Chemistry Research, 51, 14135–14144.

Reverberi, A., Fabiano, B., Cerrato, C., Dovì, V., 2014. Concentration polarization in reverse osmosis membranes: Effect of membrane splitting. Chemical Engineering Transaction, 39, 763–768.

Sannino, D., Saccoa, O., Chianese, A., 2013. Determination of optimal operating condition in nanofiltration (NF) and reverse osmosis (RO) during the treatment of a tannery wastewater stream. Chemical Engineering Transaction, 23, 1993–1998.

Sarkar, P., Goswami, D., Prabhakar, S., Tewari, P.K., 2008. Optimized design of a reverse osmosis system with a recycle. Desalination, 230, 128–139.

Sassi, K.M., Mujtaba, I.M., 2013. Optimal operation of RO system with daily variation of freshwater demand and seawater temperature. Computers and Chemical Engineering, 59, 101–110.

Senthilmurugan, S., Ahluwalia, A., Gupta, S.K., 2005. Modeling of a spiral-wound module and estimation of model parameters using numerical techniques. Desalination, 173, (3), 269–286.

Sharma, V.K., 2012. Kinetics and mechanism of formation and destruction of N nitrosodimethylamine in water- A review. Separation and Purification Technology, 88, 1–10.

Song, L., Hong, S., Hu, J., Ong, S., Ng, W., 2002. Simulations of Full-Scale Reverse Osmosis Membrane Process. Journal of Environmental Engineering, 128, 10, 960.

Spiegler, K.S., Kedem, O., 1966. Thermodynamics of hyperfiltration (reverse osmosis): criteria for efficient membranes. Desalination, 1, 311–326.

Steinle-Darling, E., Zedda, M., Plumlee, M. H., Ridgway, H. F., Reinhard, M., 2007. Evaluating the impacts of membrane type, coating, fouling, chemical properties and water chemistry on reverse osmosis rejection of seven nitrosoalklyamines, including NDMA. Water Research, 41 (17) 3959–3967.

Thomson, M., Miranda, M.S., Infield, D., 2002. A small-scale seawater reverse-osmosis system with excellent energy efficiency over a wide operating range. Desalination, 153, 229–236.

US EPA, 2009a. United States Environmental Protection Agency IRIS database, https://www.epa.gov/iris.

US EPA, 2009b. Contaminant Information Sheets for the Final CCL 3 Chemicals, EPA.

Villafafila, A., Mujtaba, I.M., 2003. Fresh water by reverse osmosis based desalination: simulation and optimisation. Desalination, 155, l–13.

Voros, N., Maroulis, Z.B., Marinos-Kouris, D., 1997. Short-cut structural design of reverse osmosis desalination plants. J. Membr. Sci., 127(1) 47–68.

Wagner J., 2001. Membrane filtration handbook practical tips and hints. Second Edition, Revision 2. Osmonics, Inc.

Zhu, A., Christofides, P.D., Cohen, Y., 2009. Effect of Thermodynamic Restriction on Energy Cost Optimisation of RO Membrane Water Desalination. Industrial and Engineering Chemistry Research, 48, 6010–6021.

Appendix A

Table A. 1. Spiral-wound reverse osmosis modelling of Al-Obaidi et al. (2017b)

Model Equations		Eq. no.
$F_{b(x)} = \dfrac{F_{b(L)}\left(e^{\sqrt{\frac{L_p}{Z}}x} - e^{-\sqrt{\frac{L_p}{Z}}x}\right) + F_{b(0)}\left(e^{\sqrt{\frac{L_p}{Z}}(L-x)} - e^{-\sqrt{\frac{L_p}{Z}}(L-x)}\right)}{\left(e^{\sqrt{\frac{L_p}{Z}}L} - e^{-\sqrt{\frac{L_p}{Z}}L}\right)}$		1
Where, $Z = \dfrac{1 + \frac{\sigma\, C_{p(av)}\, L_{p(T_b)}}{\omega_{(T_b)}} - \frac{\tilde{C}_{s(av)}(1-\sigma)\, L_{p(T_b)}\, \sigma}{\omega_{(T_b)}}}{W\, b}$		2
$\omega = \dfrac{B_s}{R\,(T_b+273.15)}$		3
$\tilde{C}_{s(av)} = \dfrac{\tilde{C}_{s(0)} + \tilde{C}_{s(L)}}{2}$		4
Where, $\tilde{C}_{s(0)} = \dfrac{C_{s(0)} - C_{p(av)}}{\ln\left(\frac{C_{s(0)}}{C_{p(av)}}\right)}$ and $\tilde{C}_{s(L)} = \dfrac{C_{s(L)} - C_{p(av)}}{\ln\left(\frac{C_{s(L)}}{C_{p(av)}}\right)}$		5,6
$F_{b(L)} = \dfrac{F_{b(0)}\left(e^{\sqrt{\frac{L_p}{Z}}L} + e^{-\sqrt{\frac{L_p}{Z}}L}\right)}{2} - \dfrac{\Delta P_{b(0)}\sqrt{\frac{L_p}{Z}}\left(e^{\sqrt{\frac{L_p}{Z}}L} + e^{-\sqrt{\frac{L_p}{Z}}L}\right)}{2b}$		7
$U_{b(x)} = \dfrac{F_{b(x)}}{t_f\, W}$		8
$P_{b(x)} = P_{b(0)} - \dfrac{b}{\sqrt{\frac{L_p}{Z}}\left(e^{\sqrt{\frac{L_p}{Z}}L} - e^{-\sqrt{\frac{L_p}{Z}}L}\right)}\left\{\left[F_{b(L)}\left[e^{\sqrt{\frac{L_p}{Z}}x} + e^{-\sqrt{\frac{L_p}{Z}}x} - 2\right] - F_{b(0)}\left[\left(e^{\sqrt{\frac{L_p}{Z}}(L-x)} + e^{-\sqrt{\frac{L_p}{Z}}(L-x)}\right) - \left(e^{\sqrt{\frac{L_p}{Z}}L} - e^{-\sqrt{\frac{L_p}{Z}}L}\right)\right]\right]\right\}$		9
$\Delta P_{b(x)} = \dfrac{\sqrt{\frac{L_p}{Z}}\, Zb\left\{\left[F_{b(0)}\left(e^{\sqrt{\frac{L_p}{Z}}(L-x)} + e^{-\sqrt{\frac{L_p}{Z}}(L-x)}\right)\right] - \left[F_{b(L)}\left(e^{\sqrt{\frac{L_p}{Z}}x} + e^{-\sqrt{\frac{L_p}{Z}}x}\right)\right]\right\}}{L_p\left(e^{\sqrt{\frac{L_p}{Z}}L} - e^{-\sqrt{\frac{L_p}{Z}}L}\right)}$		10
$J_{w(x)} = \dfrac{\sqrt{\frac{L_p}{Z}}}{W\left(e^{\sqrt{\frac{L_p}{Z}}L} - e^{-\sqrt{\frac{L_p}{Z}}L}\right)}\left\{\left[F_{b(0)}\left(e^{\sqrt{\frac{L_p}{Z}}(L-x)} + e^{-\sqrt{\frac{L_p}{Z}}(L-x)}\right)\right] - \left[F_{b(L)}\left(e^{\sqrt{\frac{L_p}{Z}}x} + e^{-\sqrt{\frac{L_p}{Z}}x}\right)\right]\right\}$		11
$J_{s(x)} = J_{w(x)}\,(1-\sigma)\,\tilde{C}_{s(av)} + \omega_{(T_b)}\, R\, T_b\,\left(C_{w(x)} - C_{p(av)}\right)$		12
$\dfrac{\left(C_{w(x)} - C_{p(av)}\right)}{\left(C_{s(x)} - C_{p(av)}\right)} = exp\left(\dfrac{J_{w(x)}}{k_{(x)}}\right)$		13
$D_{b(x)} = 6.725E-6\ exp\left\{0.1546x10^{-3}\, C_{s(x)}\,(18.01253) - \frac{2513}{T_b+273.15}\right\}$	(Koroneos et al., 2007)	14
$\mu_{b(x)} = 1.234E-6\ exp\left\{0.0212x10^{-3}\, C_{s(x)}\,(18.0153) + \frac{1965}{T_b+273.15}\right\}$	(Koroneos et al., 2007)	15
$\rho_{b(x)} = 498.4\, m_{f(x)} + \sqrt{\left[248400\, m_{f(x)}^2 + 752.4\, m_{f(x)}\, C_{s(x)}\,(18.0153)\right]}$	(Koroneos et al., 2007)	16
$m_{f(x)} = 1.0069 - 2.757E-4\ T_b$		17
$\dfrac{d\frac{\left(C_{s(x)}\, F_{b(x)}\right)}{t_f\, W}}{dx} = -\dfrac{J_{w(x)} C_{p(av)}}{t_f} + \dfrac{J_{w(x)}\, C_{s(x)}}{t_f} + \dfrac{d}{dx}\left(D_{b(x)}\dfrac{dC_{s(x)}}{dx}\right)$		18
$C_{p(av)} = \dfrac{C_{p(0)} + C_{p(L)}}{2}$		19
$C_{p(0)} = \dfrac{B_{s(T_b)}\, R\, T_b\, C_{s(0)}\, e^{\frac{J_{w(0)}}{k_{(0)}}}}{J_{w(0)} + B_{s(T_b)}\, R\, T_b\ e^{\frac{J_{w(0)}}{k_{(0)}}}}$ and $C_{p(L)} = \dfrac{B_{s(T_b)}\, R\, T_b\, C_{s(L)}\, e^{\frac{J_{w(L)}}{k_{(L)}}}}{J_{w(L)} + B_{s(T_b)}\, R\, T_b\ e^{\frac{J_{w(L)}}{k_{(L)}}}}$		20, 21
$\dfrac{dF_{p(x)}}{dx} = -\dfrac{dF_{b(x)}}{dx}$		22
$F_{p(Total)} = F_{p(L)}$		23
$Rec_{(Total)} = \dfrac{F_{p(Total)}}{F_{b(0)}}\, x\ 100$		24
$Rej_{observed} = \dfrac{C_{b(0)} - C_{p(av)}}{C_{b(0)}}\, x100$ $\quad Rej = \dfrac{Rej_{observed}\ \exp\left(\frac{J_{w(L)}}{k_{(L)}}\right)}{1 + Rej_{observed}\left[\exp\left(\frac{J_{w(L)}}{k_{(L)}}\right) - 1\right]}$	Fujioka (2014)	25, 26